

Residual Control for Fast Recovery from Dynamics Shifts

Nethmi Jayasinghe¹, Diana Gontero¹, Francesco Migliarba¹, Spencer T. Brown², Vinod K. Sangwan³, Mark C. Hersam^{3,4,5}, Amit Ranjan Trivedi¹

Abstract—Robotic systems operating in real-world environments inevitably encounter unobserved dynamics shifts during continuous execution, including changes in actuation, mass distribution, or contact conditions. When such shifts occur mid-episode, even locally stabilizing learned policies can experience substantial transient performance degradation. While input-to-state stability guarantees bounded state deviation, it does not ensure rapid restoration of task-level performance. We address inference-time recovery under frozen policy parameters by casting adaptation as constrained disturbance shaping around a nominal stabilizing controller. We propose a stability-aligned residual control architecture in which a reinforcement learning policy trained under nominal dynamics remains fixed at deployment, and adaptation occurs exclusively through a bounded additive residual channel. A Stability Alignment Gate (SAG) regulates corrective authority through magnitude constraints, directional coherence with the nominal action, performance-conditioned activation, and adaptive gain modulation. These mechanisms preserve the nominal closed-loop structure while enabling rapid compensation for unobserved dynamics shifts without retraining or privileged disturbance information. Across mid-episode perturbations including actuator degradation, mass variation, and contact changes, the proposed method consistently reduces recovery time relative to frozen and online-adaptation baselines while maintaining near-nominal steady-state performance. Recovery time is reduced by 87% on the Go1 quadruped, 48% on the Cassie biped, 30% on the HI humanoid, and 20% on the Scout wheeled platform on average across evaluated conditions relative to a frozen SAC policy. **Demonstrations on the Agilex Scout Mini Pro are provided in the supplementary material.**

I. INTRODUCTION

Robotic systems operating outside controlled laboratory environments inevitably encounter unmodeled changes in actuation, mass distribution, or contact conditions during execution. When such dynamics shifts occur mid-episode, the performance of learned control policies can degrade abruptly. In practical deployments, recovery must occur online without resetting the system, retraining the controller, or accessing privileged disturbance information. At the same time, modifying a learned policy during execution risks perturbing the closed-loop structure that underlies nominal stability and long-horizon competence. The central challenge

is therefore enabling rapid inference-time recovery from unobserved dynamics shifts while preserving the stabilizing behavior of a frozen learned policy. This setting is common in practical deployments where policies are pre-trained offline and runtime modification of policy parameters is undesirable due to safety, certification, or compute constraints.

Even when a nominal policy remains locally stabilizing under moderate parameter variation, abrupt shifts can induce substantial transient performance loss. Input-to-state stability (ISS) guarantees bounded state deviation but does not ensure rapid restoration of task-level performance. In many robotic applications, recovery speed following a disturbance or fault is as critical as steady-state stability. The problem is therefore not only maintaining bounded behavior, but minimizing recovery time under frozen policy parameters and unknown post-shift dynamics.

Existing approaches address runtime perturbations in three primary ways. Robust reinforcement learning internalizes parameter variation during training [1], [2], [3], but the resulting controller remains fixed at deployment and does not explicitly optimize recovery speed. Test-time adaptation and meta-learning update policy parameters online [4], [5], [6], altering the closed-loop mapping and potentially disrupting learned stabilization structure. Classical adaptive control and disturbance-observer methods modify gains or estimate parameters within the controller itself [7], [8], typically relying on structural assumptions that are difficult to guarantee for high-dimensional learned policies. In all cases, adaptation occurs inside the primary control law, coupling recovery dynamics with nominal stabilization.

Biological motor control offers an alternative architecture. In vertebrate motor systems, motor programs generated by cortical and brainstem pathways produce baseline actions, while the cerebellum operates as a parallel adaptive module that injects rapid corrective refinements without overwriting the primary controller. Input expansion in granule-cell layer provides a fixed high-dimensional basis [9], Plasticity at Purkinje cell synapses adapts corrections through error-driven updates [10], and cerebellar output nuclei regulate corrective authority based on task-level error signals. Critically, these corrections act additively on the motor command rather than reparameterizing the nominal control policy, thereby enabling rapid compensation for unexpected perturbations while preserving stable baseline behavior.

Motivated by this principle, we treat a reinforcement learning policy trained under nominal dynamics as a stabilized baseline controller that remains fixed at deployment. Adaptation is realized through a parallel residual channel that injects

¹Department of Electrical and Computer Engineering, University of Illinois at Chicago, Chicago, IL, USA.

²Department of Neurobiology, Northwestern University, Evanston, IL, USA.

³Department of Materials Science and Engineering, Northwestern University, Evanston, IL, USA.

⁴Department of Electrical and Computer Engineering, Northwestern University, Evanston, IL, USA.

⁵Department of Chemistry, Northwestern University, Evanston, IL, USA.

Correspondence: Nethmi Jayasinghe (wjayas3@uic.edu), Amit Ranjan Trivedi (amitr@uic.edu).

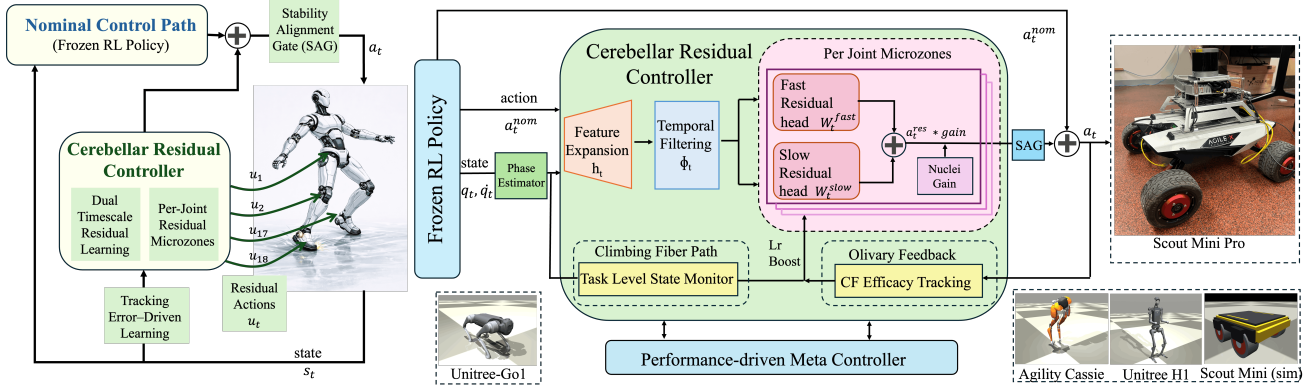


Fig. 1. Overview of the proposed cerebellar-inspired residual control architecture. A frozen RL policy provides nominal control, while a parallel cerebellar residual controller generates per-joint residual actions via microzone-based pathways. Tracking-error driven learning updates dual-timescale residual heads online for rapid adaptation. A Stability Alignment Gate (SAG) constrains residual magnitude and directional alignment before combining the residual with the nominal policy to produce the final action a_t .

bounded corrective actions in action space. The residual does not modify policy parameters, critics, or latent representations; instead, it enters the closed loop as a regulated additive disturbance. A Stability Alignment Gate (SAG) constrains corrective authority through magnitude bounds, directional coherence with the nominal action, performance-conditioned activation, and adaptive gain modulation. These mechanisms preserve the nominal closed-loop structure while enabling rapid compensation for unobserved dynamics shifts.

Across quadrupedal, bipedal, humanoid, and wheeled platforms, the proposed architecture significantly accelerates recovery following mid-episode perturbations. Recovery time is reduced by up to 87%, 48%, 30%, and 20% on the Go1 quadruped, Cassie biped, H1 humanoid, and Scout wheeled platform, respectively, relative to a frozen SAC baseline, while maintaining near-nominal steady-state performance. We additionally validate the framework on a physical AgileX Scout Mini Pro platform.

II. RELATION TO PRIOR WORK

Robustness and runtime adaptation in robotics have been studied through robust training, online parameter estimation, meta-learning, and classical adaptive control. In most existing approaches, adaptation is internalized during training or embedded inside the controller through weight or gain updates at deployment. In contrast, our approach separates stabilization and adaptation by introducing a bounded residual channel operating around a frozen policy, enabling recovery without modifying the nominal controller.

Robust Reinforcement Learning. Domain randomization and adversarial training [1], [2], [3] improve robustness by exposing policies to parameter variation during training. While effective within the training distribution, the resulting controller remains fixed at deployment and does not explicitly optimize recovery dynamics when unexpected shifts occur mid-episode.

Online Identification and Meta-Adaptation. Methods such as RMA, OSI, MAML, PEARL, and test-time training [11], [12], [13], [4], [5] adapt policies online through latent parameter inference or gradient-based updates. Although these

approaches enable rapid adaptation, they modify the policy itself during execution, altering the closed-loop mapping and potentially disrupting learned stabilization structure. In contrast, our method keeps the nominal policy fixed and performs adaptation exclusively through an external residual channel without explicit system identification.

Adaptive Control and Robust MPC. Classical adaptive control techniques such as MRAC and RLS, as well as disturbance observers [7], estimate model parameters or update control gains online under structural assumptions such as known model form or persistent excitation. Robust MPC incorporates uncertainty sets directly into optimization-based feedback. These methods embed adaptation inside the controller and rely on modeling assumptions that are often difficult to satisfy for high-dimensional learned policies.

Residual and Cerebellar-Inspired Architectures. Residual policy learning augments a nominal controller with corrective actions [14], while cerebellar-inspired models emphasize parallel error-driven correction layered onto baseline motor programs [9], [10], [15], [16]. However, prior residual approaches typically train corrective policies offline or lack mechanisms to regulate corrective authority during deployment. In contrast, our method learns residual corrections online at inference time while enforcing bounded, stability-aligned authority constraints that preserve the nominal closed-loop under unexpected dynamics shifts.

III. METHODOLOGY

A. Problem Formulation and Control Objective

Consider a robotic system with state $s_t \in \mathcal{S}$ and control input $a_t \in \mathcal{A}$ evolving under parameterized dynamics

$$s_{t+1} = f(s_t, a_t; \omega_t), \quad (1)$$

where $\omega_t \in \Omega$ denotes physical parameters such as actuator gains, mass distribution, or contact properties. During training, $\omega_t = \omega^*$, and a policy π_θ is optimized under the nominal closed loop

$$s_{t+1} = f(s_t, \pi_\theta(s_t); \omega^*). \quad (2)$$

Assumption 1 (Local Robust ISS). There exists a neighborhood $\mathcal{W} \subset \Omega$ containing ω^* such that for all $\omega \in \mathcal{W}$ the closed loop induced by π_θ is locally input-to-state stable (ISS) around an invariant manifold \mathcal{M} and achieves baseline performance level J^* .

Justification. Learned locomotion policies are typically trained to stabilize trajectories around a gait manifold \mathcal{M} under bounded disturbances and modeling noise. Empirically, such policies exhibit local robustness to moderate variations in actuation, mass distribution, and contact properties. We therefore restrict attention to perturbations within a local robustness region \mathcal{W} around ω^* , where trajectories remain bounded and nominal task performance is preserved. This assumption characterizes the regime in which residual adaptation operates and does not imply global robustness.

At deployment, an abrupt and unobserved parameter shift occurs at time τ , with $\omega_t = \omega^*$ for $t < \tau$ and $\omega_t = \tilde{\omega} \neq \omega^*$ for $t \geq \tau$. The goal is to restore task performance without modifying the nominal policy. The deployed controller is therefore restricted to the additive form

$$a_t = \pi_\theta(s_t) + u_t, \quad (3)$$

where u_t is generated online during execution.

Let \bar{J}_t denote a smoothed performance signal and J^* the nominal performance level. For tolerance $\delta > 0$, define the recovery time

$$T_\delta := \inf \{t \geq \tau \mid \bar{J}_t \geq J^* - \delta\}. \quad (4)$$

The objective is to design the residual correction u_t that minimizes T_δ under unknown post-shift dynamics $\tilde{\omega}$ while preserving the stabilizing structure of the nominal controller. To ensure that adaptation operates within the robustness margin of the base policy, corrective authority is bounded, $\|u_t\|_2 \leq \varepsilon$, so that the adapted system can be interpreted as the nominal closed loop driven by a bounded disturbance. This formulation shifts the adaptation problem from policy reparameterization to disturbance shaping around a fixed stabilizing controller.

B. Cerebellar-Inspired Principles for Residual Control

Robotic deployment requires policies that remain stable under nominal dynamics while adapting to unobserved perturbations. Existing approaches rely on test-time fine-tuning and online updates [17], [6], meta-learned rapid adaptation [4], [5], or classical adaptive control and disturbance observers that modify gains or estimate latent parameters within the controller [8], [7]. Because adaptation occurs inside the primary control law, these methods can perturb the nominal closed loop or rely on identification assumptions.

Biological motor control adopts a different architectural strategy. Nominal motor programs remain intact while the cerebellum injects parallel corrective refinements [18], [19]. This separation between stabilization and correction enables rapid compensation for unexpected perturbations without overwriting the primary controller.

We adopt this structural principle directly. The learned policy π_θ serves as the nominal stabilizing controller, while adaptation occurs through a parallel residual channel:

$$a_t = a_t^{\text{nom}} + u_t, \quad a_t^{\text{nom}} := \pi_\theta(s_t), \quad (5)$$

$$u_t = \gamma_t(\beta_t \odot a_t^{\text{res}}), \quad (6)$$

where $a_t^{\text{res}} \in \mathbb{R}^d$ denotes the residual output, $\gamma_t \in \mathbb{R}_+$ controls global corrective authority, and $\beta_t \in \mathbb{R}_+^d$ provides per-joint amplification. The residual does not modify policy parameters, critics, or latent representations; instead it acts as an additive correction around the nominal controller. Corrective authority is explicitly bounded,

$$\|u_t\|_2 \leq \varepsilon, \quad |u_{t,j}| \leq \varepsilon_j, \quad (7)$$

ensuring that adaptation operates within the robustness margin of the nominal closed loop rather by reparameterizing.

Transient-Sensitive Feature Encoding. Following an unobserved parameter shift $\omega^* \rightarrow \tilde{\omega}$, deviations from nominal behavior appear as transient mismatches between expected and realized state evolution. Because $\tilde{\omega}$ is unknown and system identification is not performed, the residual pathway must infer corrective structure directly from observable errors.

To amplify shift-induced deviations while suppressing steady-state behavior, we employ a fixed high-dimensional nonlinear expansion

$$h_t = \sigma(Vx_t), \quad (8)$$

where x_t denotes state-reference inputs and $V \in \mathbb{R}^{p \times m}$ is fixed. This design mirrors cerebellar circuitry in which granule cells provide a fixed basis expansion and learning occurs through downstream readout weights. By fixing V and adapting only residual weights, representation is separated from plasticity and adaptation reduces to error-driven reweighting of a rich but static feature basis.

To emphasize transients, paired temporal traces are applied

$$\phi_t^E = (1 - \alpha_E)\phi_{t-1}^E + \alpha_E h_t, \quad (9)$$

$$\phi_t^I = (1 - \alpha_I)\phi_{t-1}^I + \alpha_I h_t, \quad (10)$$

$$\phi_t = \phi_t^E - \phi_t^I, \quad (11)$$

with $0 < \alpha_I < \alpha_E < 1$. This band-pass filtering isolates rapid post-shift deviations while attenuating nominal steady-state components, producing transient-sensitive features that accelerate reduction of the recovery time T_δ .

Dual-Timescale Residual Generator. Following the transient-sensitive encoding, the residual must reduce recovery time T_δ without inducing instability or long-term drift. Biological cerebellar circuits exhibit multi-timescale plasticity in which rapid correction is followed by slower consolidation. We implement this principle using two adaptive linear heads

$$a_t^{\text{res}} = W_t^{\text{fast}}\phi_t + W_t^{\text{slow}}\phi_t, \quad (12)$$

where $W_t^{\text{fast}}, W_t^{\text{slow}} \in \mathbb{R}^{d \times p}$ evolve online with decay rates satisfying $\lambda_f > \lambda_s$. Although algebraically equivalent to a single linear map, the separation is dynamical rather than

representational. The fast head provides high-gain transient compensation immediately after a dynamics shift, while the slow head integrates persistent structure under $\tilde{\omega}$ and stabilizes adaptation once transients decay.

Online Error-Driven Plasticity. Residual adaptation is driven by task-relevant tracking error

$$e_t = \dot{q}_t^{\text{ref}} - \dot{q}_t + \Lambda(q_t^{\text{ref}} - q_t), \quad (13)$$

where $\Lambda \succeq 0$ is diagonal. Residual weights are updated according to

$$\Delta W_t \propto e_t \phi_t^\top, \quad (14)$$

with a larger learning rate assigned to the fast head to accelerate transient compensation. To prevent over-adaptation, the learning rate is modulated by a task-level error measure

$$\epsilon_t = w_p |e_t^{\text{pitch}}| + w_r |e_t^{\text{roll}}| + w_z |e_t^{\text{height}}|. \quad (15)$$

When ϵ_t exceeds a predefined threshold, learning intensity increases to amplify corrective adaptation; as performance stabilizes, the learning rate decays. This adaptive plasticity mechanism enables rapid post-shift correction while limiting parameter drift during steady-state operation.

C. Stability Alignment and Authority Regulation

The residual architecture in Sec. III-B enables rapid inference-time adaptation. However, unconstrained residual corrections may interfere with the nominal stabilizing controller π_θ . The goal is therefore not only fast adaptation but *stability-aligned adaptation*, where corrective authority increases under degradation while remaining bounded and consistent with the nominal closed loop. To enforce this property we introduce the *Stability Alignment Gate (SAG)*, which regulates when/how residual corrections are injected.

Stability Alignment Gate (SAG). Corrective authority is regulated through four coupled mechanisms:

(1) *Magnitude constraints.* Residual injection is bounded,

$$\|u_t\|_2 \leq \varepsilon, \quad |u_{t,j}| \leq \varepsilon_j, \quad (16)$$

ensuring that adaptation enters the closed loop as a bounded disturbance rather than a structural controller modification.

(2) *Directional coherence.* Residual components that oppose the nominal control direction are attenuated to prevent destructive interference with stabilizing actions.

(3) *Performance-conditioned activation.* Corrective authority increases only after sustained degradation in the smoothed performance signal \bar{J}_t , preventing unnecessary intervention during nominal operation.

(4) *Adaptive gain regulation.* Global and per-joint amplification factors γ_t and β_t expand under persistent tracking error and contract as performance recovers.

The following subsections describe the implementation of these mechanisms:

Directional Coherence Implementation. Residual corrections should reinforce, rather than oppose, stabilizing control directions produced by π_θ . Since the nominal policy is assumed to remain locally stabilizing within the robustness

neighborhood \mathcal{W} , persistent opposition by the residual may reduce effective feedback gain or introduce oscillatory behavior. To quantify alignment, we compute the cosine similarity

$$c_t = \frac{\langle a_t^{\text{nom}}, a_t^{\text{res}} \rangle}{\|a_t^{\text{nom}}\|_2 \|a_t^{\text{res}}\|_2 + \xi}, \quad (17)$$

with $\xi > 0$ for numerical stability. A negative c_t indicates that the residual produces action components opposing the nominal control direction.

When $c_t < 0$, residual authority is attenuated:

$$u_t \leftarrow \rho(c_t) u_t, \quad \rho(c_t) = \begin{cases} 1, & c_t \geq 0, \\ \kappa, & c_t < 0, \end{cases} \quad (18)$$

with $\kappa \in [0, 1)$. This soft alignment constraint preserves corrective flexibility while preventing systematic cancellation of stabilizing torques.

Gain Regulation Dynamics. The global authority parameter γ_t determines how strongly the residual channel influences the control signal. It increases when task performance degrades and decreases as recovery occurs:

$$\gamma_t = \text{clip}_{[0, \gamma_{\max}]} \left(\gamma_{\min} + k_\gamma \frac{J^* - \bar{J}_t}{J^* - J_{\min} + \xi} \right). \quad (19)$$

Here J_{\min} denotes the running minimum of \bar{J}_t observed after the detected performance drop, providing normalization relative to the worst observed degradation. When \bar{J}_t falls far below nominal performance J^* , γ_t increases, allowing stronger corrective action. As performance recovers, γ_t contracts toward γ_{\min} .

Per-joint amplification $\beta_{t,j}$ further adjusts corrective authority locally:

$$\beta_{t+1,j} = \text{clip}_{[\beta_{\min}, \beta_{\max}]} (\beta_{t,j} + k_\beta \mathbb{I}\{|e_{t,j}| > \bar{e}_j\}). \quad (20)$$

Thus joints exhibiting sustained tracking error receive increased corrective emphasis. Both γ_t and β_t are clipped to preserve the residual magnitude bounds.

Task-Modulated Plasticity Coupling. Beyond regulating residual magnitude, SAG also modulates how aggressively residual parameters adapt. The fast-head learning rate evolves according to

$$\eta_f(t) = \eta_f^0 (1 + b_t), \quad (21)$$

$$b_{t+1} = \text{clip}_{[0, b_{\max}]} (\rho_b b_t + \alpha_b \mathbb{I}\{\epsilon_t > \bar{\epsilon}\}), \quad (22)$$

where ϵ_t is a task-level error proxy.

When sustained degradation is detected ($\epsilon_t > \bar{\epsilon}$), the boost variable b_t increases and temporarily amplifies learning intensity. As performance stabilizes, b_t decays toward zero, returning the adaptation rate to its nominal value η_f^0 .

This mechanism prevents two common failure modes of adaptive residual schemes: slow recovery due to fixed low gains and parameter drift caused by persistently high adaptation rates. By coupling plasticity directly to observed task degradation, learning intensity becomes state-dependent rather than constant.

TABLE I

GoI recovery performance under representative perturbations. Metrics include recovery AUC, SSR, TTR-50, and total return (mean \pm std over 30 trials). Higher is better for AUC, SSR, and total return; lower is better for TTR-50.

Category	Method	Actuator Degradation (0.76 \times)				Mass Increase (1.15 \times)				Friction Increase (2.1 \times)			
		AUC \uparrow	SSR \uparrow	Recovery Steps \downarrow	TotalR \uparrow	AUC \uparrow	SSR \uparrow	Recovery Steps \downarrow	TotalR \uparrow	AUC \uparrow	SSR \uparrow	Recovery Steps \downarrow	TotalR \uparrow
No Adapt	SAC-Only	0.437	0.427	4500	9562 \pm 122	1.001	1.001	1950	18411 \pm 104	0.934	0.933	4500	17233 \pm 115
	SAC + Ours	0.664	0.666	3962	13520 \pm 150	1.042	1.044	168	20150 \pm 295	0.973	0.965	173	18783 \pm 143
Online	SAC + MRAC	0.372	0.392	2442	8439 \pm 3719	0.908	0.904	2929	17778 \pm 1498	0.496	0.445	4361	10595 \pm 1807
	SAC + RLS	0.402	0.462	2230	8961 \pm 3443	0.918	0.912	2553	17957 \pm 1619	0.529	0.443	4102	11164 \pm 3447
	Online SAC	0.384	0.243	3802	8651 \pm 3511	0.716	0.558	3813	14432 \pm 3159	0.432	0.325	4356	9470 \pm 2450
Fault-Aware	OSI	0.555	0.554	4500	13458 \pm 1410	0.991	0.987	3556	22289\pm145	0.972	0.967	4500	21895\pm144
	RMA	0.642	0.639	4500	15208 \pm 2954	0.975	0.972	4500	21923 \pm 1131	0.892	0.886	4500	20246 \pm 1031
	DR-SAC	0.571	0.384	3778	9578 \pm 3168	0.902	0.903	3334	14204 \pm 118	0.429	0.286	3727	7562 \pm 1481
	PEARL	0.907	0.908	3512	18260\pm73	0.964	0.964	2886	19282 \pm 71	0.869	0.869	4500	17593 \pm 70
	RARL	1.056	1.075	2260	10425 \pm 2388	0.511	0.472	2867	6086 \pm 4267	0.656	0.650	2711	6889 \pm 2618
	RPL	0.716	0.717	3590	13591 \pm 170	1.014	1.013	1834	18490 \pm 133	0.894	0.894	2290	16519 \pm 131

Stability Interpretation: Under SAG, the adapted closed loop evolves as

$$s_{t+1} = f(s_t, \pi_\theta(s_t) + u_t; \tilde{\omega}), \quad \|u_t\|_2 \leq \varepsilon. \quad (23)$$

Thus the residual correction acts as a bounded exogenous input to the nominal closed-loop system.

Let the distance to the invariant set \mathcal{M} be defined as

$$\text{dist}(s, \mathcal{M}) = \inf_{y \in \mathcal{M}} \|s - y\|_2.$$

Under Assumption 1 (Local Robust ISS), the nominal closed loop induced by π_θ is locally input-to-state stable around \mathcal{M} for all $\omega \in \mathcal{W}$. Therefore there exist functions $\alpha \in \mathcal{K}$ and $\beta \in \mathcal{KL}$ such that, for all trajectories remaining in the local robustness neighborhood,

$$\text{dist}(s_t, \mathcal{M}) \leq \beta(\text{dist}(s_0, \mathcal{M}), t) + \alpha\left(\sup_{0 \leq k \leq t} \|u_k\|_2\right).$$

Because SAG enforces $\|u_t\|_2 \leq \varepsilon$, the deviation from the invariant set remains bounded within the robustness region. Residual adaptation therefore operates *around* the stabilizing controller rather than modifying it internally.

Overall, SAG imposes three structural constraints: bounded residual authority, activation only under sustained performance degradation, and directional alignment with the nominal controller. These constraints ensure that adaptation reshapes recovery dynamics while preserving the stabilizing structure of the nominal closed loop.

IV. EXPERIMENTAL SETUP

Simulation Platform: Experiments are conducted in MuJoCo [20]. The primary platform is a 12-DOF quadruped trained for forward locomotion under torque control. The state includes joint positions, velocities, and body pose features, while actions correspond to normalized joint torques.

Nominal Policy: The nominal controller is a Soft Actor-Critic (SAC) [21] policy trained under nominal dynamics ω^* and frozen at deployment. During evaluation no policy retraining, system identification, reset-based recovery, or privileged disturbance information is permitted.

Mid-Episode Perturbation Protocol: Each rollout lasts 5000 simulation steps. A dynamics shift is injected at step 500 and maintained thereafter. We evaluate three perturbation families: actuator scaling, mass variation, and friction change. Each family contains six severity levels (18 total conditions). Every condition is evaluated on 30 trials.

Evaluation Metrics: Recovery behavior is quantified using four metrics: (i) *TTR-50*, the number of steps required for the exponentially smoothed reward to recover 50% of the post-fault drop; (ii) *Recovery AUC*, the normalized post-fault reward trajectory; (iii) *Steady-State Ratio (SSR)*, the normalized reward during the final phase of the rollout; and (iv) *Total Episode Reward*. Values of AUC or SSR greater than 1.0 indicate post-fault performance exceeding the nominal baseline.

Baselines: We compare against frozen SAC (no adaptation), online SAC updates, classical adaptive control methods (MRAC, RLS), and robustness-through-training approaches including DR-SAC, RMA, OSI, PEARL, RARL, and RPL. All methods are evaluated under the same mid-episode perturbation protocol without reset-based recovery.

V. RESULTS

A. Quantitative Comparison on Unitree GoI

Table I reports recovery performance on the Unitree GoI under actuator, mass, and friction perturbations. The proposed stability-aligned residual controller consistently achieves the fastest recovery while maintaining competitive steady-state performance, often reducing recovery time by an order of magnitude relative to frozen and online-adaptation.

Under actuator degradation (0.76 \times), fault-aware methods achieve strong steady-state metrics due to disturbance exposure during training. Our method remains competitive in AUC and SSR while outperforming non-fault-aware online baselines, preserving stable behavior without privileged disturbance information. Under mass increase (1.15 \times), separation is pronounced: the proposed controller restores task performance within 168 steps, whereas most baselines require thousands of steps or fail to recover within the episode horizon. Steady-state performance remains above

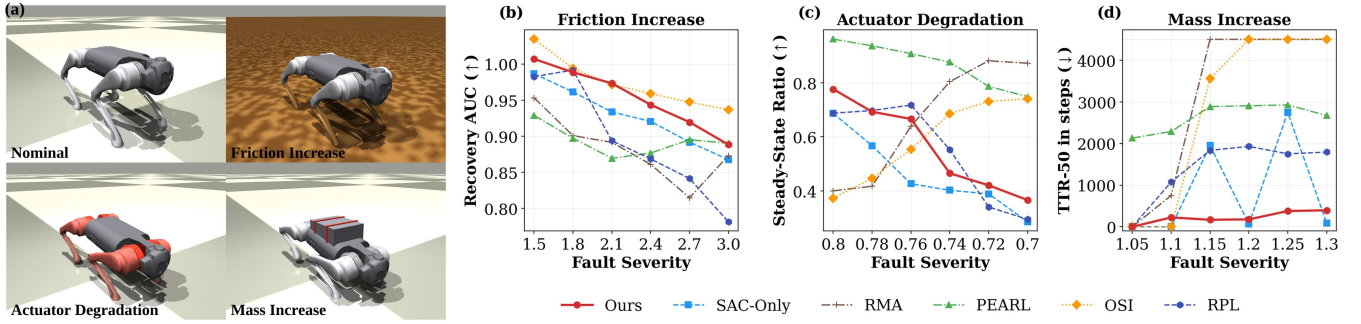


Fig. 2. Performance under mid-episode perturbations on the Go1 quadruped across increasing fault severities. (a) Friction increase: Recovery AUC (\uparrow). (b) Actuator degradation: Steady-State Ratio (\uparrow). (c) Mass increase: Time-to-Recovery (TTR-50, \downarrow). Averaged over 30 trials per condition. The proposed method achieves faster recovery while preserving competitive steady-state performance across perturbation types.

TABLE II

Cross-platform recovery performance on Agility Cassie (biped) and Unitree H1 (humanoid). Metrics include time-to-recovery at 50% (TTR-50), steady-state ratio (SSR), and total episode return (TotalR \pm std over 30 trials). Lower is better for TTR-50; higher is better for SSR and TotalR.

Category	Method	Agility Cassie						Unitree H1					
		Mass (1.15 \times)			Friction (1.4 \times)			Mass (1.15 \times)			Friction (1.3 \times)		
		SSR \uparrow	TTR-50 \downarrow	TotalR \uparrow	SSR \uparrow	TTR-50 \downarrow	TotalR \uparrow	SSR \uparrow	TTR-50 \downarrow	TotalR \uparrow	SSR \uparrow	TTR-50 \downarrow	TotalR \uparrow
No Adaptation	SAC-Only	1.037	1351	16755 \pm 2042	0.958	2800	15568 \pm 458	1.064	298	24548 \pm 123	1.060	465	24396 \pm 109
Online	SAC + Ours	1.077	601	17219 \pm 1484	1.171	142	18234 \pm 442	1.065	116	25546 \pm 124	1.061	373	25453 \pm 112
	SAC + MRAC	1.073	611	17151 \pm 844	1.071	957	17477 \pm 746	1.062	392	25512 \pm 134	1.096	427	25784 \pm 245
	SAC + RLS	1.061	1051	16968 \pm 1101	1.101	354	17749 \pm 732	1.063	505	25419 \pm 124	1.069	436	25842\pm177
Fault-Aware	OSI	0.844	2162	16147 \pm 3709	0.812	2822	17070 \pm 2083	0.931	2967	23128 \pm 1099	1.039	1966	23495 \pm 731
	RMA	0.986	3900	16912 \pm 4419	0.951	2942	18870\pm2873	1.057	350	24573 \pm 233	1.057	379	23633 \pm 400
	DR-SAC	1.070	594	17268\pm127	1.082	151	17573 \pm 119	1.060	334	23509 \pm 1545	1.041	2043	23165 \pm 209

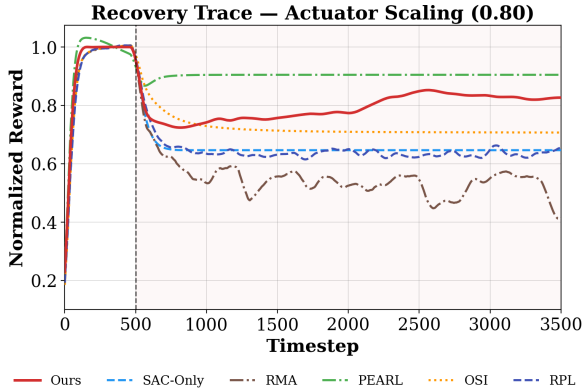


Fig. 3. Normalized reward traces following mid-episode mild actuator degradation (scaling factor 0.80) on the Go1 quadruped. The fault is injected at timestep 500.

nominal levels (SSR $>$ 1.0), indicating that rapid transient correction does not degrade long-horizon behavior. Under friction increase (2.1 \times), the proposed method again achieves the fastest recovery (173 steps), while competing approaches recover substantially slower or incompletely.

Overall, these results show that separating stabilization and adaptation through a bounded residual channel enables rapid inference-time recovery while preserving the nominal policy structure, without retraining or disturbance exposure.

B. Scaling Across Fault Severities

Figs. 2–3 illustrate recovery dynamics and scaling behavior as fault severity increases. Fig. 3 shows the full reward trajectories following mid-episode fault injection. All methods experience an abrupt performance drop at the perturbation time, but the subsequent recovery behavior differs substantially. The proposed controller exhibits the steepest recovery slope and smooth convergence toward nominal reward. In contrast, several baselines display slow recovery, large oscillations, or persistent performance degradation. In many cases recovery remains incomplete within the horizon.

Fig. 2 analyzes how recovery degrades as perturbation severity increases. Across all fault families, the proposed controller shows controlled and gradual degradation rather than abrupt performance collapse. Under friction increase (Fig. 2b), recovery AUC decreases smoothly for all methods as severity grows. However, the proposed controller maintains consistently high AUC values across the entire sweep, while several baselines degrade sharply at higher friction.

Under actuator degradation (Fig. 2c), steady-state ratios decline with decreasing torque authority. Fault-aware methods perform competitively at moderate severity due to disturbance exposure during training. The proposed controller remains stable and competitive across the full scaling range without privileged disturbance information.

Mass increase (Fig. 2d) produces the clearest separation. For the proposed controller, TTR-50 grows gradually with severity and remains within hundreds of steps. In contrast,

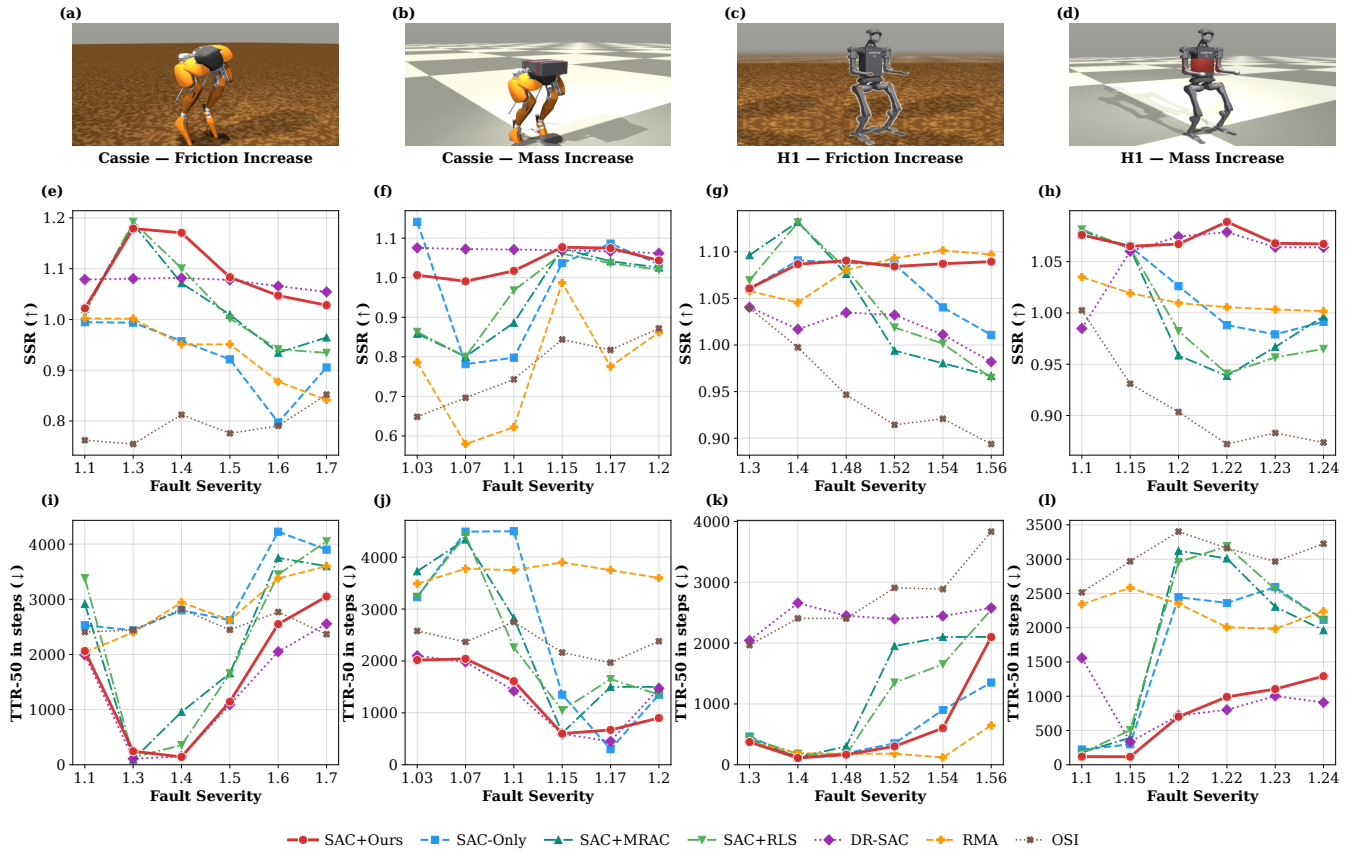


Fig. 4. Cassie and H1 evaluation under mid-episode perturbations. (a,b) Cassie under friction and mass increase. (c,d) H1 under friction and mass increase. (e-h) Steady-state stability ratio (SSR; higher is better) versus fault severity. (i-l) Recovery time (TTR-50; lower is better) for the same conditions. The proposed stability-aligned residual controller consistently reduces recovery time while maintaining near-nominal steady-state performance across bipedal and humanoid platforms.

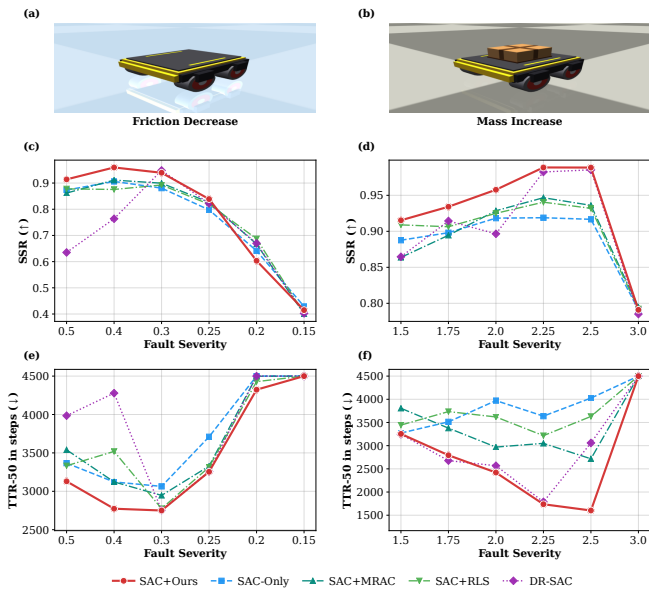


Fig. 5. Scout platform evaluation under mid-episode perturbations. (a,b) Friction decrease and mass increase scenarios. (c,d) Steady-state stability ratio (SSR; higher is better) versus fault severity. (e,f) Recovery time (TTR-50; lower is better) for the same conditions. The proposed stability-aligned residual controller improves recovery speed while preserving steady-state stability across perturbations.

most baselines scale into thousands of recovery steps or fail

to recover within the episode horizon. This behavior indicates that the proposed residual controller degrades gracefully under progressively larger dynamics shifts than collapsing.

C. Cross-Platform Evaluation

We evaluate structural generality across platforms with distinct contact regimes, dimensionality, and control interfaces. Representative comparisons are shown in Table II, with severity scaling in Fig. 4 (Cassie, H1) and Fig. 5 (Scout).

Agility Cassie (Biped). Cassie exhibits hybrid contact transitions with narrow stability margins. Table II shows substantial recovery acceleration. Under mass increase ($1.15\times$), TTR-50 decreases from 1351 (SAC-only) to 601 steps while SSR improves from 1.037 to 1.077. Under friction increase ($1.4\times$), recovery time drops from 2800 to 142 steps with steady-state performance preserved (SSR $0.958\rightarrow 1.171$). Fig. 4 shows similar trends across severities, with gradual degradation rather than abrupt instability.

Unitree H1 (Humanoid). The 19-DOF H1 introduces higher dimensionality and reduced stability margins. As shown in Table II, recovery time improves consistently (e.g., $298\rightarrow 116$ steps under mass increase) while SSR remains near nominal. Fig. 4 confirms smooth scaling of both SSR and TTR-50 with increasing severity, indicating stable adaptation in high-dimensional whole-body control.

TABLE III

Ablation study on Go1 under mass increase (1.15 \times), 30 trials. Lower TTR-50 is better; higher TotalR and AUC are better.

	Full	No CF	No Dual-Head	No Olivary	No Nuclei Gate	No Dir. Align	No Temp. Filt.
TTR-50 \downarrow	168	171	186	273	174	3367	1127
AUC \uparrow	1.042	1.040	1.039	1.041	1.003	1.021	1.023
SSR \uparrow	1.044	1.042	1.005	1.040	1.002	1.018	1.024
TotalR \uparrow	20150\pm295	20006 \pm 297	19971 \pm 276	20140 \pm 294	20143 \pm 294	19762 \pm 526	19793 \pm 136

Agilex Scout (Wheeled Platform). The Scout Mini represents a velocity-controlled platform with continuous ground contact and different disturbance propagation dynamics. Fig. 5 shows consistently faster recovery across mass and friction perturbations relative to frozen SAC, while steady-state performance remains comparable. Performance separation is strongest under moderate perturbations and saturates near actuator limits. Across hybrid-contact bipeds, high-DOF humanoids, and wheeled systems, the proposed method consistently accelerates recovery while preserving steady-state performance, indicating that stability-aligned residual adaptation generalizes across diverse robot morphologies.

Thus, because the residual channel operates purely in action space and does not depend on robot-specific dynamics models, the same adaptation mechanism transfers across platforms without architectural modification.

D. Ablation Study

We evaluate component contributions on Go1 under a representative mass increase (1.15 \times) perturbation (Table III). The results reveal a clear hierarchy of importance. For example, removing directional alignment causes severe degradation (TTR-50: 168 \rightarrow 3367) and reduces total reward. Without alignment, residual actions can oppose stabilizing torques from the nominal policy, effectively reducing closed-loop damping. This confirms that directional coherence acts as a structural stability constraint rather than a performance refinement. Removing transient-sensitive temporal filtering also significantly slows recovery (168 \rightarrow 1127). Without band-pass isolation, adaptation responds to steady-state components instead of shift-induced transients, diluting corrective authority. In contrast, removing dual-timescale decomposition (168 \rightarrow 186), nuclei gain modulation (168 \rightarrow 174), or CF tracking (168 \rightarrow 171) produces only moderate degradation, indicating that these components primarily refine convergence dynamics. Removing the olivary pathway increases TTR-50 to 273, suggesting slower consolidation while preserving stable behavior.

Thus two key insights emerge from the above analysis: *First*, mechanisms regulating where and when residual authority is applied are more critical than those governing adaptation rate. *Second*, stability-aligned constraints dominate representational complexity. Even a simple linear residual remains effective when bounded and aligned, whereas unconstrained correction destabilizes recovery. This suggests that enforcing stability-aligned constraints is more important than increasing representational capacity in the residual module.

VI. CONCLUSION

We proposed a cerebellar-inspired stability-aligned residual controller for rapid inference-time recovery of learned robotic policies under unobserved dynamics shifts. The method injects bounded residual corrections around a frozen nominal controller, enabling fast recovery without policy updates or system identification. Experiments across multiple robot platforms demonstrate consistently faster recovery with near-nominal steady-state performance, with ablations highlighting the roles of directional alignment, transient-sensitive filtering, and dual-timescale adaptation.

REFERENCES

- [1] J. Tobin, R. Fong, A. Ray, J. Schneider, W. Zaremba, and P. Abbeel, "Domain randomization for transferring deep neural networks from simulation to the real world," in *2017 IEEE/RSJ international conference on intelligent robots and systems (IROS)*. IEEE, 2017, pp. 23–30.
- [2] L. Pinto, J. Davidson, R. Sukthankar, and A. Gupta, "Robust adversarial reinforcement learning," in *International conference on machine learning*. PMLR, 2017, pp. 2817–2826.
- [3] X. B. Peng, M. Andrychowicz, W. Zaremba, and P. Abbeel, "Sim-to-real transfer of robotic control with dynamics randomization," in *2018 IEEE international conference on robotics and automation (ICRA)*. IEEE, 2018, pp. 3803–3810.
- [4] C. Finn, P. Abbeel, and S. Levine, "Model-agnostic meta-learning for fast adaptation of deep networks," in *International conference on machine learning*. PMLR, 2017, pp. 1126–1135.
- [5] K. Rakelly, A. Zhou, C. Finn, S. Levine, and D. Quillen, "Efficient off-policy meta-reinforcement learning via probabilistic context variables," in *International conference on machine learning*. PMLR, 2019, pp. 5331–5340.
- [6] D. Wang, E. Shelhamer, S. Liu, B. Olshausen, and T. Darrell, "Tent: Fully test-time adaptation by entropy minimization," in *International Conference on Learning Representations*, 2021. [Online]. Available: <https://openreview.net/forum?id=uX13bZLkr3c>
- [7] P. A. Ioannou and J. Sun, *Robust adaptive control*. PTR Prentice-Hall Upper Saddle River, NJ, 1996, vol. 1.
- [8] J.-J. E. Slotine and W. Li, *Applied Nonlinear Control*. Englewood Cliffs, New Jersey: Prentice Hall, 1991.
- [9] J. S. Albus, "A theory of cerebellar function," *Mathematical Biosciences*, vol. 10, pp. 25–61, 1971.
- [10] M. Kawato and H. Gomi, "A computational model of four regions of the cerebellum based on feedback-error learning," *Biological Cybernetics*, vol. 68, no. 2, pp. 95–103, 1992.
- [11] A. Kumar, Z. Fu, D. Pathak, and J. Malik, "Rma: Rapid motor adaptation for legged robots," *arXiv preprint arXiv:2107.04034*, 2021.
- [12] W. Yu, J. Tan, C. K. Liu, and G. Turk, "Preparing for the unknown: Learning a universal policy with online system identification," *arXiv preprint arXiv:1702.02453*, 2017.
- [13] Y. Qiu, X. Lin, J. Wang, X. Li, L. Qi, and M.-H. Yang, "Umc: Unified resilient controller for legged robots with joint malfunctions," 2025. [Online]. Available: <https://arxiv.org/abs/2502.03035>
- [14] T. Johannink, S. Bahl, A. Nair, J. Luo, A. Kumar, M. Loskyll, J. A. Ojea, E. Solowjow, and S. Levine, "Residual reinforcement learning for robot control," in *2019 international conference on robotics and automation (ICRA)*. IEEE, 2019, pp. 6023–6029.
- [15] J. S. Albus, "A new approach to manipulator control: The cerebellar model articulation controller (cmac)," *Journal of Dynamic Systems, Measurement, and Control*, vol. 97, no. 3, pp. 220–227, 1975.

- [16] N. Jayasinghe, D. Gontero, S. T. Brown, V. K. Sangwan, M. C. Hersam, and A. R. Trivedi, "Cerebellar-inspired residual control for fault recovery: From inference-time adaptation to structural consolidation," 2026. [Online]. Available: <https://arxiv.org/abs/2602.07227>
- [17] Y. Sun, X. Wang, Z. Liu, J. Miller, A. Efros, and M. Hardt, "Test-time training with self-supervised optimizations," in *International Conference on Machine Learning (ICML)*. PMLR, 2020, pp. 9213–9224.
- [18] D. M. Wolpert, R. C. Miall, and M. Kawato, "Internal models in the cerebellum," *Trends in Cognitive Sciences*, vol. 2, no. 9, pp. 338–347, 1998.
- [19] M. Ito, "Control of mental activities by internal models in the cerebellum," *Nature Reviews Neuroscience*, vol. 9, no. 4, pp. 304–313, 2008.
- [20] E. Todorov, T. Erez, and Y. Tassa, "Mujoco: A physics engine for model-based control," in *2012 IEEE/RSJ International Conference on Intelligent Robots and Systems*. IEEE, 2012, pp. 5026–5033.
- [21] T. Haarnoja, A. Zhou, P. Abbeel, and S. Levine, "Soft actor-critic: Off-policy maximum entropy deep reinforcement learning with a stochastic actor," in *Proceedings of the 35th International Conference on Machine Learning (ICML)*, 2018, pp. 1861–1870.